Investigation of Microstructure and Dielectric Behavior of Bi2/3Cu3-xMgxTi4O12(x=0, 0.05, 0.1 and 0.2) Ceramics Synthesized by Semi-Wet Route

Vishnu Shankar Rai
Indian Institute of Technology BHU Varanasi
Santosh Pandey
Indian Institute of Technology BHU Varanasi
Vinod Kumar
Indian Institute of Technology BHU Varanasi
Manish Kumar Verma
Indian Institute of Technology BHU Varanasi
Atendra Kumar
Indian Institute of Technology BHU Varanasi
Shruti Singh
Indian Institute of Technology BHU Varanasi
Dinesh Prajapati
Indian Institute of Technology BHU Varanasi
Prof. K.D. Mandal (kdmandal.apc@itbhu.ac.in)
Indian Institute of Technology (BHU) Varanasi

Research Article

Keywords: Semi-wet route, Microstructural Studies, Dielectric properties, Impedance properties, XPS

Posted Date: August 26th, 2020

DOI: https://doi.org/10.21203/rs.3.rs-64822/v1

Investigation of microstructure and dielectric behavior of $Bi_{2/3}Cu_{3-x}Mg_xTi_4O_{12}$(x=0, 0.05, 0.1 and 0.2) ceramics synthesized by semi-wet route

Vishnu Shankar Rai, Santosh Pandey, Vinod Kumar, Manish Kumar Verma, Atendra Kumar, Shruti Singh, Dinesh Prajapati, K.D. Mandal*

Department of Chemistry, Indian Institute of Technology (Banaras Hindu University), Varanasi- 221005, U.P. India

Abstract

In this manuscript, We have reported the synthesis and characterization of Mg-doped and undoped BCTO ceramic ($Bi_{2/3}Cu_{3-x}Mg_xTi_4O_{12}$, x=0,0.05,0.1,0.2) sintered at 1173 K for 8 h, which have been prepared by the semi-wet path. Single-phase formation of ceramic was approved by the XRD pattern. The Microstructural properties were studied by TEM and AFM. The samples were characterized by dielectric and impedance spectroscopic properties. The dielectric constant (ε_r) was calculated to be 3024 for BCTO ceramics at 423 K and 100 Hz. The tangent loss (tan δ) value was calculated to be 0.45 for BCTO ceramic at 423 K and 10 kHz. The internal Barrier Layer Capacitance (IBLC) mechanism was responsible for the high value of dielectric constant. XPS spectroscopy confirmed the oxidation state of the ceramic. It was observed from Impedance and modulus studies that there was the existence of the Maxwell-Wagner form of relaxation in the ceramics.

Keyword – Semi-wet route, Microstructural Studies, Dielectric properties, Impedance properties, XPS.

*Corresponding author

Email address:-kdmandal.apc@itbhu.ac.in

1.Introduction

$ACu_3Ti_4O_{12}$ (where A =Ca, $Y_{2/3}$, $Bi_{2/3}$, $Gd_{2/3}$) type of perovskite oxide was the first time revealed in 1967 [1], which was able to produce high dielectric constant. The detection of ultrahigh dielectric response in body-centered $CaCu_3Ti_4O_{12}$(CCTO) has been induced vast research to understand the underlying physics behind the unusual phenomenon [2]. For many technical uses such as condensers, resonators, filters, and memory chips, high dielectric materials have been fascinated very much [3-5]. Regularly, the size and execution of such electronic gadgets can be managed by their material properties. Further, the dielectric consistent of the material should be independent of temperature and frequency [6]. Recently, high dielectric permittivity ($\varepsilon \sim 10^4$)with weakly temperature and frequency-dependent permittivity have been noticed in TiO_2–based ceramics and CCTO ($CaCu_3Ti_4O_{12}$)-like compounds [7]. The search for ultrahigh permittivity ($\varepsilon_r > 10^3$) materials is one of the most popular research topics in the fields of microelectronics and energy storage devices.$CaCu_3Ti_4O_{12}$(CCTO), a typical $ACu_3Ti_4O_{12}$ (ACTO, where A = Ca, Cd, $La_{2/3}$, $Y_{2/3}$, $Bi_{2/3}$, $Na_{1/2}La_{1/2}$, $Na_{1/2}Y_{1/2}$, or $Na_{1/2}Bi_{1/2}$, Sr) ceramic, has been widely studied due to its ultrahigh dielectric permittivity and good frequency/thermal stability. However, other members of the ACTO family with isostructures, have also been widely studied. Impedance spectroscopy estimation shows that the high dielectric steady is a direct result of the Internal Barrier Layer Capacitance (IBLC) impact [8-13]. $Bi_{2/3}Cu_3Ti_4O_{12}$(BCTO) is isostructural with CCTO, has been reported in the literature. It indicated the temperature and frequency dependence of dielectric as CCTO [14-16].. Particles covered with a thin coating of other materials have improved properties compared to non-functional uncoated particles, such as the Lu3Al5O12.Ce@SiO2 core-shell composite, which reduced the thermal/chemical degradation of LEDs [18]. Because of their possible applications in various fields such as engineered multiferroics, catalysts, and biomedical applications, core-shell structured materials have been mostly studied for a few years [17]. The sources of high permittivity in ACTO materials would

include extrinsic processes. According to this reasoning, an IBLC model, i.e. semi-conducting grains separated by isolating grain boundaries, is currently the most accepted way to explain this phenomenon [19-21]. Polarisation at the interfaces of the substance electrodes may also lead to this extrinsic effect [24]. The reasons behind the presence of semiconductivity in the bulk, however, are not yet clear. Cation non-stochiometry mechanism relating to a Cu deficiency in the interior grain area was alleged to responsible for this effect [22-24].In this present study, We have reported the effects of Mg doping on Cu sites on dielectric properties and Impedance studies of BCTO Ceramic, which was synthesized through the semi-wet method. Its microstructure, dielectric and electric properties were described.

2. Material Synthesis

$Bi_{2/3}Cu_{3-x}Mg_xTi_4O_{12}$ (where x=0, 0.05, 0.1, 0.2) was synthesized through semi-wet method.For x=0, the formula becomes $Bi_{2/3}Cu_3Ti_4O_{12}$ and the sample is abbreviated as BCTO. For x=0.05, the formula becomes $Bi_{2/3}Cu_{2.95}Mg_{0.05}Ti_4O_{12}$ and the sample is abbreviated as BCMgTO-0.05. For x=0.1, the formula becomes $Bi_{2/3}Cu_{2.9}Mg_{0.1}Ti_4O_{12}$ and the sample is abbreviated as BCMgTO-0.1. For x=0.2, the formula becomes $Bi_{2/3}Cu_{2.8}Mg_{0.2}Ti_4O_{12}$ and the sample is abbreviated as BCMgTO-0.2. In this technique, chemicals Bismuth nitrate $Bi(NO_3)_3{\cdot}5H_2O$ (99%Merck, India), copper acetate $Cu(CH_3COO)_2{\cdot}H_2O$ (99% Merck, India), magnesium acetate $Mg(CH_3COO)_2{\cdot}H_2O$ (98.5% Merck, India), and titanium oxide TiO_2 (98.5% Merck, India) starting were used in the stoichiometric ratio. The solution of $Bi(NO_3)_3.5H_2O$, $Cu(CH_3COO)_2{\cdot}H_2O$, and $Mg(CH_3COO)_2{\cdot}H_2O$ was prepared in distilled water. Solid TiO_2 was added to this solution. The stoichiometric amount of citric acid (99.5%, Merck India) as a chelating agent, was dissolved in distilled water and combined with the solution. The resultant solution was heated on a hot plate magnetic stirrer at 343-353 K to vaporize water permitted for self-ignition. A fluffy mass of BCTO and BCMgTO powders were obtained after the removal of a lot of gasses. Citric acid was also applied as fuel in the ignition step. The resulting BCTO and BCMgTO powders were ground with the help of pestle

and mortar to make a fine powder. The powders were calcined at 1073 K for 6 h. Cylindrical pellets were made with calcined powders using 2% PVA as a binder on applying 5 tons of pressure using hydraulic pressure for 90 s. This binder was burnt out at 773 K for 3 h. Finally, the BCTO and BCMgTO pellets were sintered at 1173 K for 8 h.

3.Material Characterization

The crystalline phase of the sintered samples was identified by using X-ray Diffractometer (MiniFlex2 goniometer, Rigaku, Tokyo, Japan under 30Kv/15mAX-Ray,2θ/θ-continuous scanning mode within the scanning range 20-90°) technique employing CuK_{α} radiation (λ=1.54059Å). Bright Field TEM images were obtained by transmission electron microscopy (TEM, FEI Tecnai-20 G) with an accelerating voltage of 200 kV. Samples were characterized also by XPS(X-ray Photoelectron Spectroscopy) and AFM (Atomic Force Microscopy). For dielectric measurements, sintered pellets were polished by silver paste both sides and dielectric data were taken by LCR meter (PSM 1735-NumetriQ, Newton 4th Ltd.UK) with a variation of temperature and frequency.

4.Results and discussion

4.1. X-ray diffraction (XRD) Analysis

X-ray diffraction pattern of Mg doped and undoped BCTO ceramics $Bi_{2/3}Cu_{3-x}Mg_xTi_4O_{12}$(where x=0, 0.05,0.1,0.2) sintered at 1173 K for 8 h is presented in figure 1, which clearly shows BCTO phase(JCPDS card no. 46-0725).The main XRD diffraction peaks of BCTO ceramic corresponding to (2 1 1),(2 2 0),(3 1 0),(2 2 2),(3 2 1), (4 0 0), (4 2 2), (4 4 0) planes were found to have the same as CCTO (JCPDS card no. 75-2188).

The crystalline size (D) of BCTO and BCMgTO ceramics was determined using the Debye-Scherrer's formula:- $$D = \frac{k\lambda}{\beta cos\theta} \quad \ldots\ldots(1)$$

where k is the crystal shape coefficient (k=0.89), λ is the wavelength used in XRD, β is the Full-Width Half Maximum(FWHM) and θ is the diffraction angle. The calculated value of average crystalline size for BCTO, BCMgTO-0.05, BCMgTO-0.1 and BCMgTO-0.2 ceramics were found to be 35.27 nm, 44.06 nm, 46.70 nm and 44.72 nm respectively.

4.2. Microstructural Studies

1. Transmission Electron Microscopic (TEM) studies:-

The bright-field TEM image of BCMgTO-0.2 ceramic sintered at 1173 K for 8 h is shown in fig. 2(a). The TEM image confirms that the BCTO ceramic possesses crystalline particles of cubical shape. The particle size was observed by TEM analysis with the help of Image-J software and was found to be 102.6 nm for BCMgTO-0.2 ceramic.Fig. 2(b) displays Selected Area Electron Diffraction (SAED) pattern of BCMgTO-0.2 ceramic. The occurrence of a few clear rings in the SAED pattern shows the single-phase formation of crystalline BCTO ceramic.

2. Atomic Force Microscopic (AFM) studies

Fig. 3(a) and (b) depicts the 2-D AFM image for grain and grain boundary of BCMgTO-0.2 ceramic respectively, which confirms the presence of clear grains separated by grain boundaries. The three-dimensional image of BCMgTO-0.2 ceramic is shown in fig. 3(c). The average roughness (R_a) and Root mean square roughness (R_q) was calculated by using NOVA software for a three-dimensional image and found to be $86.46\,nm$ and $109.91\,nm$ for BCMgTO-0.2 ceramic sintered at 1173 K for 8 h

respectively.Fig. 3(d) shows the histogram plots for particle size which shows that most of the roughness of particles was calculated in the range between 0.4-0.7 μm for BCMgTO-0.2 ceramic.

4.3.X-ray photoelectron spectroscopic (XPS) studies

Fig. 4(a)-(e) shows the XPS spectrum of BCMgTO-0.2 ceramic.For this analysis, Carbon 1s was taken as reference, which has assigned B.E. value 284.6eVto account for the charge effects of the surface.Fig. 4 (b) depicts the XPS spectrum of Bi in BCMgTO-0.2. Two values were achieved $^{4}f_{5/2}$ and $^{4}f_{7/2}$, whose corresponding B.E. values were 158.8 eV and 164.1 eV. The above result confirmed that bismuth ion exists in the +3oxidation state in BCMgTO-0.2 ceramic. Binding energy peak was found to be at 1303.6 eV and 1304.4 eV for Mg 1s lower and higher respectively, which is shown in Fig. 4(c). The above result confirmed the existence of a +2 oxidation state of Mg ion in the ceramic. Fig. 4(a) depicts the XPS spectrum of Copper in BCMgTO-0.2 ceramic. The binding energy of copper in BCMgTO-0.2 ceramic confirmed the existence of a +2 oxidation state of Cu with the binding energy related to Cu ^{2}p spectra at the peak of 933.9 eV and 953.6 eV that corresponds to Cu $^{2}p_{3/2}$ and Cu $^{2}p_{1/2}$, respectively [25].Fig. 4(d) depicts the XPS spectrum of BCMgTO-0.2 ceramic at 457.9 eV, 463.7 eV of BCMgTO-0.2 ceramic which corresponding to the Ti ^{2}p doublet namely Ti $^{2}p_{3/2}$ and Ti $^{2}P_{1/2}$ confirmed the presence of +4 oxidation state of Ti ion [26]. The binding energy peak of Oxygen BCMgTO-0.2 ceramic was found to be 529.6 eV and 530.9 eV corresponding to lower and higher binding energy, is shown in Fig. 4(e). The above result confirmed the presence of +2 oxidation state of Oxygen ion in BCMgTO-0.2 ceramic. Thus, all ions present in the ceramic were found in the required oxidation states, which was confirmed by XPS studies.

4.4. Dielectric studies

Fig.5.(a) displays the frequency dependence of ε_r for sintered Mg-doped and undoped BCTO ceramics at 303 K. The value of ε_r for BCTO, BCMgTO-0.05, BCMgTO-0.1, and BCMgTO-0.2 ceramics were found to be 3024,325,800 and 200 respectively at 423 K and 100 Hz. The dielectric constant (ε_r) decreases rapidly in the lower frequency range whereas, in the higher frequency range, It decreases slowly as shown in fig. 5(a). Fig. 5.(b) shows the variation of tangent loss (tanδ) with frequency at 303K. It is obvious from the figure that the value of tanδ decreases with an increase in frequency in lower frequency regions, while it decreases smoothly in the higher frequency region. The dielectric loss of BCTO, BCMgTO-0.05, BCMgTO-0.1, and BCMgTO-0.2 ceramics was found to be 0.45,0.27,0.26 and 0.28 respectively at 303 K and 10 kHz. Fig. 6(a) and fig. 6(b) displays the variation of ε_r and tangent loss with the temperature at 10 kHz frequency. It is noted from the figure that the value of ε_r and tanδ first increases, attains a maximum, and then decreases slowly to a lower value.

4.5. Impedance spectroscopic studies

The complex impedance plot (Z'' vs Z') of Mg-doped and undoped BCTO ceramics sintered at 1173 K for 8 h at 303 K is shown in fig. 7(a). The figure reveals the presence of semicircular arcs with different intercepts, which may be due to the grain and grain boundary contribution in higher frequency, and no contribution due to electrode specimens is observed in this frequency range. The arcs for grains at high frequency get suppressed due to the high value of grain boundary resistance, which is usually observed for IBLC, a characteristic of semiconducting grain with an insulating grain boundary. Thus, the dielectric property of BCTO ceramics(Mg-doped and non-doped) is due to the combined effect of grain and grain boundary. The variation of the imaginary part of impedance (Z'') and the real part of impedance(Z') with frequency at 303 K is shown in fig. 7(b) and fig. 7(c) respectively. It shows the appearance of relaxation peaks. The peaks relaxation was observed at a lower frequency and peaks suppression occurred at high frequency, which confirms the presence of the relaxation phenomenon of $Bi_{2/3}Cu_3Ti_4O_{12}$ ceramics.

4.6.Electric Modulus studies

The cole-core plot(complex impedance plot)between M'' and M' for Mg doped and undoped BCTO ceramic is shown in fig. 8(a).Semicircular arcs present in M'' vs M' plot, show grain boundaries separated by grains. This type of behavior supports the long-range reduction phenomenon. To explain the modulus spectra of BCTO ceramics (Mg-doped and undoped), the variation of imaginary and real part of electric modulus M'' and M' is plotted against frequency at 303 K and is shown in fig. 8(b) and fig. 8(c) respectively. In the low-frequency region, the magnitude of M' tends to zero, which confirms a negligibly small contribution of the electrode effect [27]. It confirms the presence of well-defined relaxation consisting of relaxation peaks. M'' vs f peaks also show dielectric relaxation. The results obtained in Modulus, coincide with impedance results.

4.7. Conductivity measurements:-

Conductivity is calculated by the following formula:-

$$\sigma = \frac{1}{R}.\left(\frac{l}{A}\right) \qquad \text{.....(2)}$$

Where σ is conductivity, R is the grain boundary resistance (ohm), lis thickness of the ceramic and A is the area of the electrode.

The variation of ln of conductivity (σ) as a function of 1000/T(K^{-1}) at 10kHz frequency for Mg-doped and non-doped BCTO ceramics sintered at 1173 Kfor 8 h, is shown in fig. 9(a). It is observed from the figure that the value of lnσ decreases with a decrease in temperature. Meanwhile, the conductivity (σ) obeys the Arrhenius law:-

$$\sigma = \sigma 0 e^{-Ea/\mathrm{kB}T} \text{.....(3)}$$

Where σ is the conductivity at the given temperature T, σ_0 is the pre-exponent factor, E_a is the activation energy, k_B is Boltzmann constant and T is the absolute temperature in K. The following relation with ln σ and 1/T can be obtained by equation (3).

$$\ln\sigma = \ln\sigma_0 - E_a/k_BT \qquad \text{.....(4)}$$

whereas conduction activation energy. Conduction activation energy as calculated by the slope of the plot of lnσ vs 1000/T. The calculated conduction activation energy values for BCTO,BCMgTO-0.05,BCMgTO-0.1 and BCMgTO-0.2ceramics are 0.27 eV, 0.16 eV,0.14eV and 0.13 eV respectively.It should be noted that by Mg doping in BCTO ceramic, its conduction activation energy decreases.

The frequency-dependent conductivity can be described by Johncher's power law, which is given by [28],

$$\sigma(\omega)=\sigma_0+A\omega^s \qquad \text{.....(5)}$$

Where A is a constant and s is the power-law exponent, $0 < s < 1$.

AC conductivity [29] mainly depends upon frequency. Variation of AC conductivity with frequency is shown in Fig. 9(b). The value of Power-law exponent(s) was calculated by the slope of $\ln\sigma_{ac}$ vs $\ln\omega$. It was calculated to be 0.94,0.89,0.64 and 0.65 for BCTO,BCMgTO-0.05,BCMgTO-0.1 and BCMgTO-0.2 ceramics respectively.

5. Conclusion

Mg-doped and undoped BCTO ceramics were successfully synthesized via a semi-wet method using metal acetate, metal nitrate solutions, and solid TiO_2 powder. BCTO phase formation was confirmed by XRD. The crystalline size of Mg-doped and non-doped BCTO ceramics were found to be in the range of 35-47 nm by XRD. The particle size of BCMgTO-0.2 ceramic(higher Mg-doped sample) was found to be

102.6 nm by TEM studies. The average Roughness (R_a) value and root mean square (R_q) value was found to be 86.46 nm and 109.91 nm respectively for BCMgTO-0.2 ceramic by AFM studies. The oxidation state was confirmed by XPS. At low frequency, a high value of dielectric constant (ε_r) and at high frequency, low tangent loss were recorded. The impedance and Modulus analysis of BCTO ceramics confirmed the presence of the phenomenon of grain and grain boundary effects. Conductivity of BCTO ceramics increases with an increase of temperature obeying Arrhenius law. AC conductivity of BCTO ceramics increases with increasing frequency satisfying Johncher's power law.

Acknowledgments

Vishnu Shankar Rai thanks Head, Department of Chemistry, IIT(BHU) Varanasi, India, for the continuation of financial assistance as DST- INSPIRE fellowship. The authors are thankful to the Incharge, CIFC, IIT(BHU) Varanasi for providing TEM, XPS, and AFM facilities.

References

[1] Santosh Pandey, Atendra Kumar, N.B.Singh, et al. Studies on dielectric and magnetic properties of $CaCu_3Ti_3MnO_{12}$ceramic synthesized via semi-wet route Journal of the Australian Ceramic Society(2019)

[2] Li, M., Cai, G., Zhang, D. F., et al. (2008). Enhanced dielectric responses in Mg-doped $CaCu_3Ti_4O_{12}$.Journal of Applied Physics, 104(7),074107

[3] Subramanian, M.A., Li, D., Duan, N., et al. High dielectric constant in $ACu_3Ti_4O_{12}$ and $ACu_3Ti_3FeO_{12}$ phases. J. Solid State Chem. 151(2), 323–325 (2000)

[4] Ramirez, A.P., Subramanian, M.A., Gardel, M., et al. Giant dielectric constant response in acopper-titanate. Solid State Commun. 115(5), 217–220 (2000)

[5] Mengjuan WU, Yingchun ZHANG, Maoqiao XIANG Synthesis, characterization and dielectric properties of a novel temperature stable (1−x)CoTiNb2O8−xZnNb2O6 ceramic Journal of Advanced Ceramics 2019, 8(2): 228–237 ISSN 2226-4108

[6] Sunita sharma,Shiv sundar yadav,M.M.Singh et al. Journal of advanced dielectrics Vol. 4, No. 4 (2014) 1450030

[7] Rai Alok Kumar, et al. "Effects of praseodymium substitution on electrical properties of $CaCu_3Ti_4O_{12}$ ceramics". Ceramics International 40.1 (2014): 181-189.

[8] C.C.Homes,T.Vogt, S.M.Shapiro et al. Optical Response of High-Dielectric-Constant Perovskite-Related Oxide Science 293(2001) 673.

[9] Sinclair, D.C., Adams, T.B., Morrison, F.D., et al. CaCu3Ti4O12 one-step internal barrier layer capacitor. Appl. Phys. Lett. 80(12), 2153–2155 (2000).

[10] T.B.Admas, D.C.Sinclair, A.R.West Giant Barrier Layer Capacitance Effects in CaCu3Ti4O12 Ceramics Adv. mater.14(2002) 1321.

[11] C. C. Homes, T. Vogt, S. M. Shapiro, et al. Charge transfer in the high dielectric constant materials CaCu3Ti4O12 and CdCu3Ti4O12 Phys. Rev. B 67, 092106.

[12] Chunlin Zhao and jiagang Wu Effects of Secondary Phases on the High-Performance Colossal Permittivity in Titanium Dioxide Ceramics ACS Applied Materials & Interfaces 2018 10 (4), 3680-3688.

[13] Suman Rani,N. Ahlawat,R. Puniab Kant,et al. Dielectric and impedance studies of La and Zn co-doped complex perovskite CaCu3Ti4O12 ceramic Ceramics International Volume 44, Issue 18, 15 December 2018, Pages 23125-23136.

[14] L Yang, G Huang, T Wang, et al. Colossal dielectric permittivity and relevant mechanism of $Bi_{2/3}Cu_3Ti_4O_{12}$ ceramics Ceramics International, 2016 – Elsevier.

[15] J.J.Liu, C.Duan, W.Yin, et al. Large dielectric constant and Maxwell–Wagner relaxation in $Bi_{2/3}Cu_3Ti_4O_{12}$, Phys. Rev.B70(2004)144106.

[16] D.R.Clarke, Varistor ceramics,J.Am.Ceram.Soc.82(1999)485–502.

[17] W. Li, R.W. Schwartz Derivation and application of an empirical formula to describe interfacial relaxation effects in homogeneous materials, J. Am. Ceram.Soc. 90 (2007) 3536.

[18] Jian Xua, Dhia A. Hassan, Ren-JieZeng, et al. Lu3Al5O12:Ce@SiO2 phosphor-in-glass: its facile synthesis, reduced thermal/chemical degradation and application in high-power white LEDs, J. Eur. Ceram. Soc. 36 (2016) 2017–2015.

[19] R. Schmidt, M.C. Stennett, N.C. Hyatt, et al. Effects of sintering temperature on the internal barrier layer capacitor (IBLC) structure in $CaCu_3Ti_4O_{12}$(CCTO)ceramics,J.Eur.Ceram.Soc.32(2012)3313e3323.

[20] D. Capsonia, M. Binia, V. Massarotti, et al. Role of doping and CuO segregation in improving the giant permittivity of $CaCu_3Ti_4O_{12}$, J. Solid State Chem. 117 (2004) 4494e4500.

[21] B.A. Bender, M.J. Pan The effect of processing on the giant dielectric propertiesof $CaCu_3Ti_4O_{12}$,Mater.Sci.Eng.B117(2005)339e347.

[22] R. L€ohnert, R. Schmidt, J. T€opfer Effect of sintering conditions on microstructure and dielectric properties of $CaCu_3Ti_4O_{12}$ (CCTO) ceramics, J. Electroceram. 34,(2015) 241-248.

[23] M. Li, D.C. Sinclair, A.R. West Extrinsic origins of the apparent relaxorlikebehavior in $CaCu_3Ti_4O_{12}$ ceramics at high temperatures: a cautionary tale, J. Appl. Phys. 109 (2011) 0841061e0841068.

[24] S.I.R. Costa, M. Li, J.R. Frade, et al. Modulus spectroscopy of $CaCu_3Ti_4O_{12}$Ceramics: clues to the internal barrier layer capacitance mechanism, RSC Adv.(2013) 7030e7036.

[25] S. Jaiswar, K.D. Mandal Evidence of enhanced oxygen vacancy defects inducing ferromagnetism in multiferroic $CaMn_7O_{12}$ manganite with sintering time, J. Phys.Chem. C 121 (2017) 19586–19601.

[26] C.S. Han, H.R. Choi, H.J. Choi, Y.S. Cho, Origin of abnormal dielectric behavior and chemical states in amorphous $CaCu_3Ti_4O_{12}$ thin films on a flexible polymer substrate, Chem. Mater. 29 (2017) 5915–5921.

[27] F.S. Howell, R.A. Bose,P.B. Macedo, et al. Electrical relaxation in a glass-forming molten salt J. Phys. Chem. 78, 639 (1974) [28] M. M. Costa, G. F. M. Pires, A. J. Terezo, et al. Impedance and modulus studies of magnetic ceramic oxide $Ba_2Co_2Fe_{12}0_{22}(Co_2Y)$ doped with Bi_2O_3J. Appl. Phys. 110, 034107 (2011).

[29] S.B.R.S.Adnan, N.S.Mohamed AC conductivity and dielectric studies of modified Li4SiO4 ceramic electrolytes Ceramics International Volume 40, Issue 7, Pages 11441-11446.

CAPTIONS OF FIGURES

Fig. 1 XRD Pattern of BCTO, BCMgTO-0.05, BCMgTO-0.1, and BCMgTO-0.2 ceramics sintered at 1173 K for 8 h.

Fig. 2 (a) Bright-field TEM image and (b) SAED pattern of BCMgTO-0.2 ceramic sintered at 1173 K for 8 h.

Fig. 3 (a) Three-dimensional image for surface roughness, (b) 2D image for grain, (c) 2D image for grain boundaries, and (d) Histogram of three-dimensional particle roughness of BCMgTO-0.2 ceramic sintered at 1173 K for 8 h.

Fig. 4 XPS spectra of (a) Cu (b) Bi (c) Mg (d) Ti (e) O of BCMgTO-0.2 ceramic sintered at 1173 K for 8 h.

Fig. 5 Frequency dependence of (a) dielectric constant(ε_r) and (b) dielectric loss ($\tan\delta$) for BCTO, BCMgTO-0.05, BCMgTO-0.1 and BCMgTO-0.2 ceramics sintered at 1173 K for 8 h.

Fig. 6 Temperature dependence of (a) dielectric constant(ε_r) and (b) tangent loss ($\tan\delta$) of BCTO, BCMgTO-0.05, BCMgTO-0.1 and BCMgTO-0.2 ceramics sintered at 1173 K for 8 h.

Fig. 7 (a) Complex impedance plot or cole-cole plot (Z'' vs Z'),(b) frequency dependence of imaginary part of impedance (Z'') and (c) frequency dependence of real part of impedance(Z') at 303 K for BCTO, BCMgTO-0.05, BCMgTO-0.1, and BCMgTO-0.2 ceramics.

Fig. 8 (a) complex electric modulus or Cole-Cole plot(M'' vs M'),(b) Frequency dependence of imaginary part of electric modulus(M'') and (c) Frequency dependence of real part of electric modulus(M') at 303 K for BCTO, BCMgTO-0.05, BCMgTO-0.1, and BCMgTO-0.2 ceramics.

Fig. 9 (a) plots of conductivity(lnσ) with the inverse of temperature at 10 kHz and (b) frequency dependence of AC conductivity at 303 K for BCTO, BCMgTO-0.05, BCMgTO-0.1, and BCMgTO-0.2 ceramics.

Figures

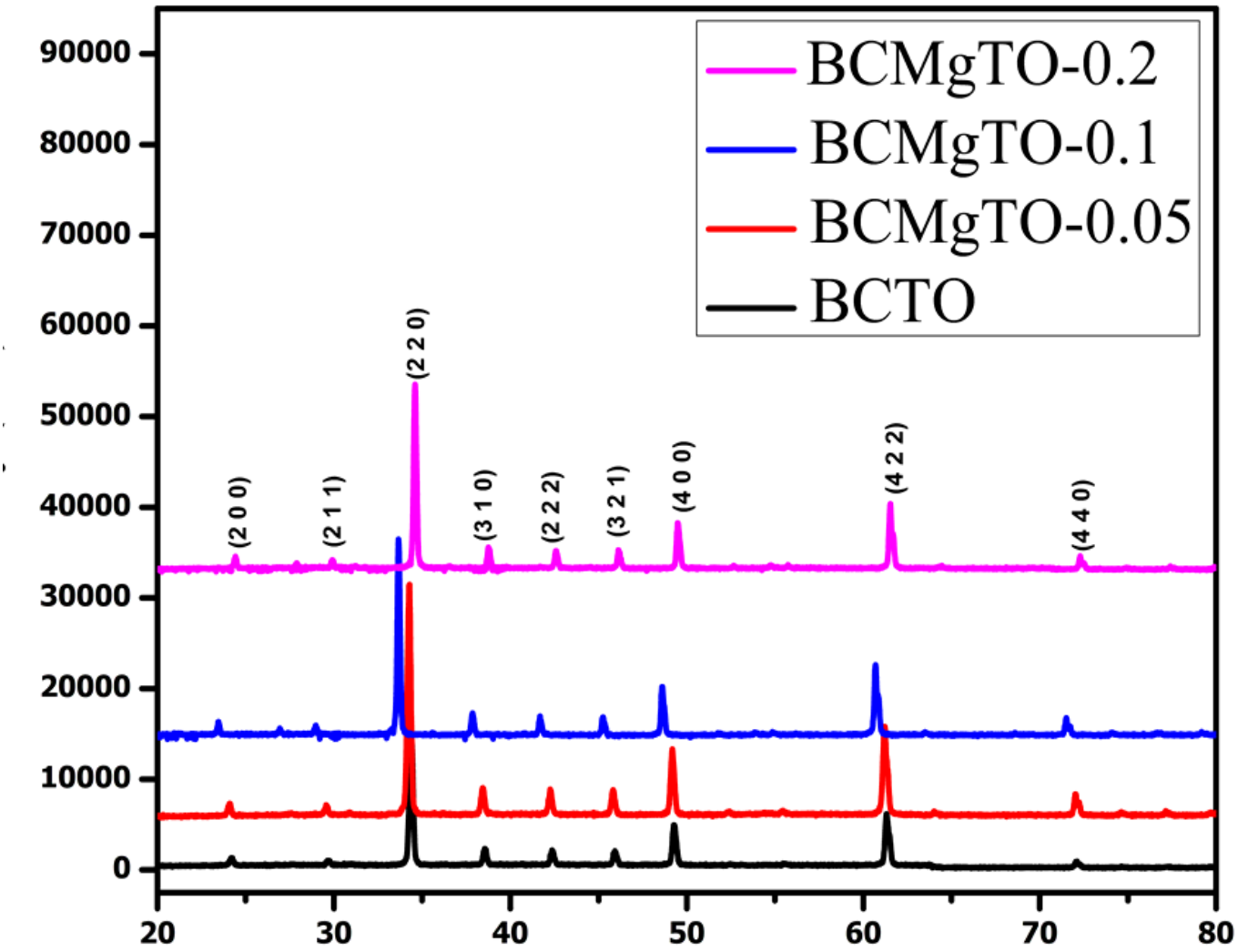

Figure 1

XRD Pattern of BCTO, BCMgTO-0.05, BCMgTO-0.1, and BCMgTO-0.2 ceramics sintered at 1173 K for 8 h.

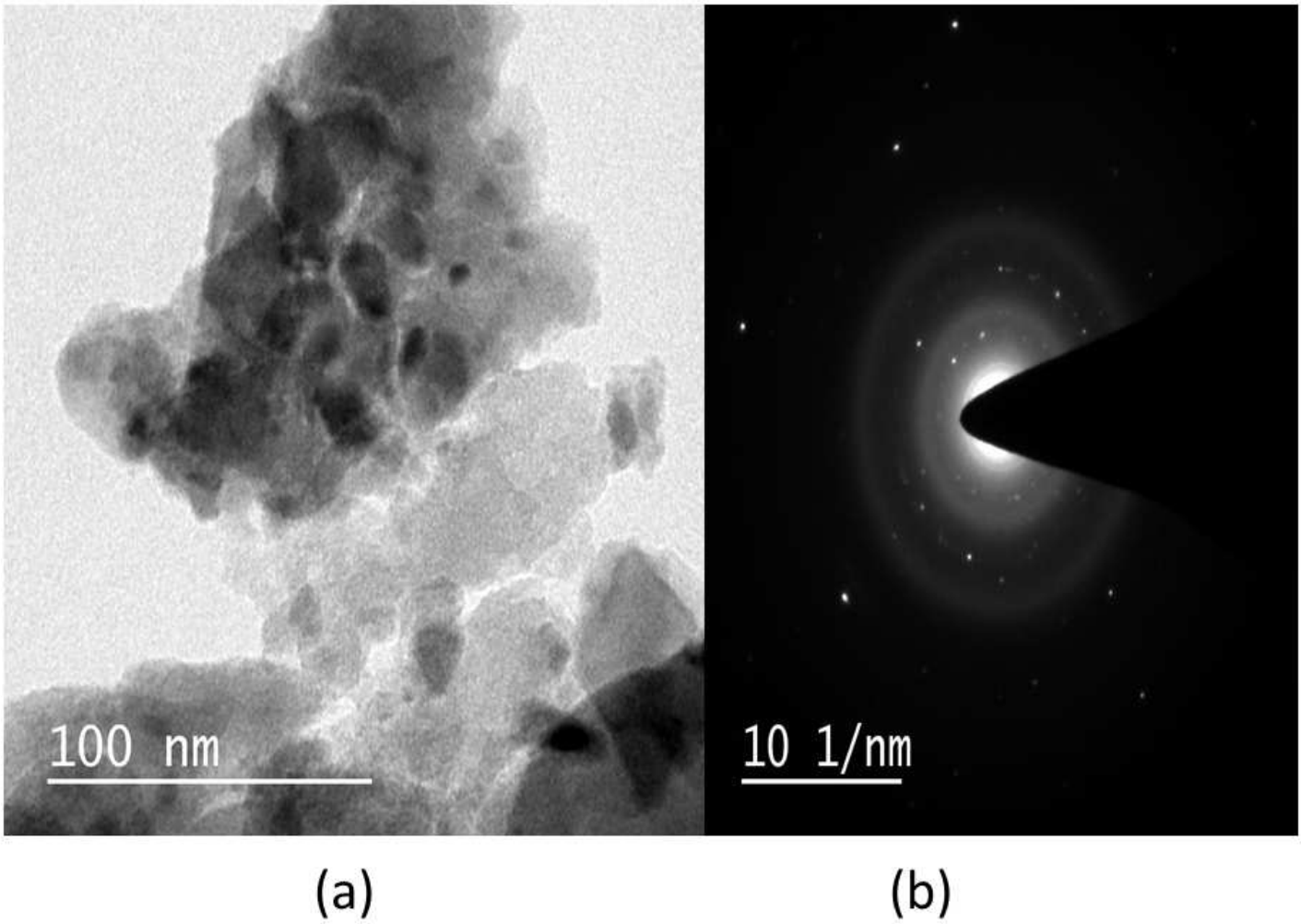

Figure 2

(a) Bright-field TEM image and (b) SAED pattern of BCMgTO-0.2 ceramic sintered at 1173 K for 8 h.

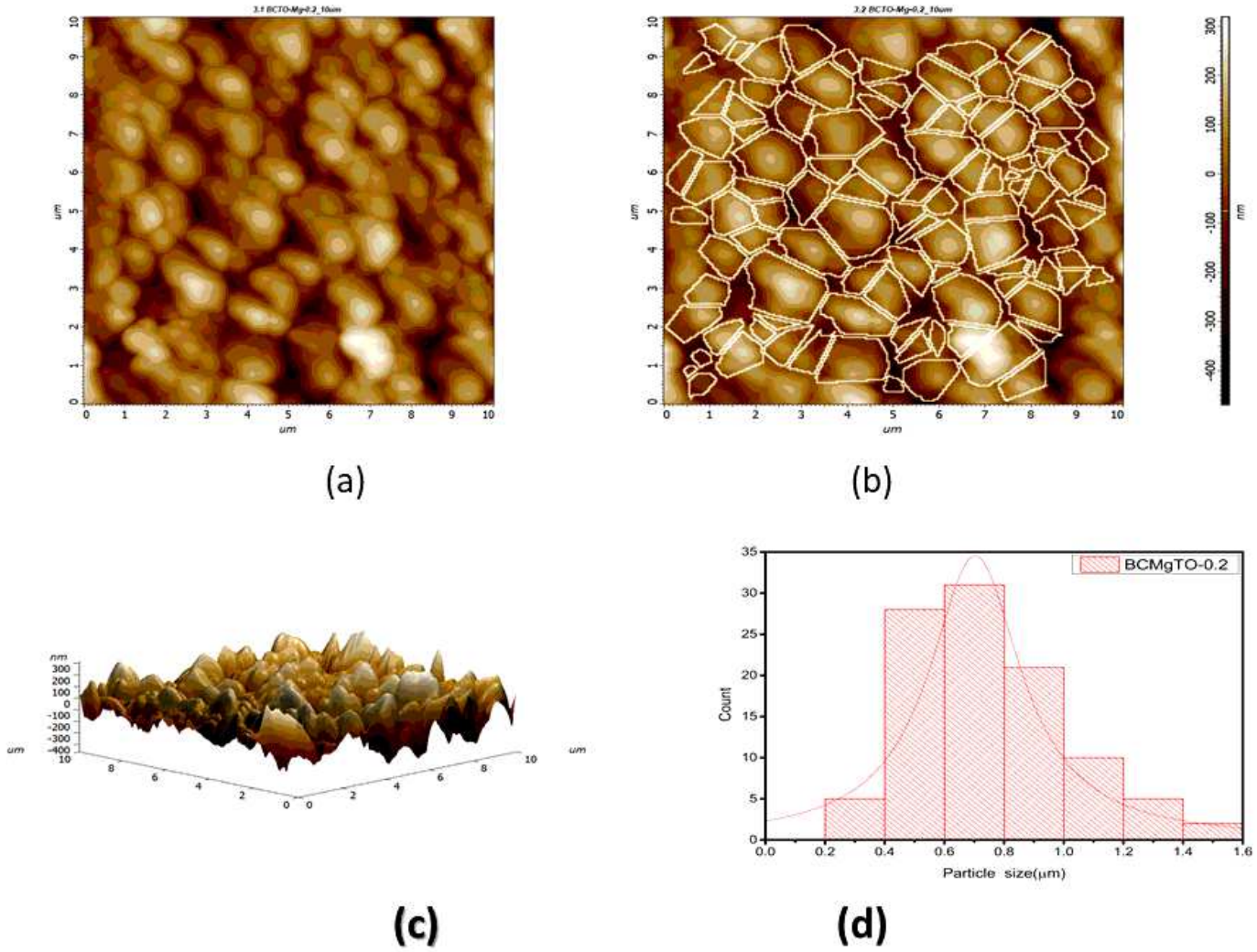

Figure 3

(a) Three-dimensional image for surface roughness, (b) 2D image for grain, (c) 2D image for grain boundaries, and (d) Histogram of three-dimensional particle roughness of BCMgTO-0.2 ceramic sintered at 1173 K for 8 h.

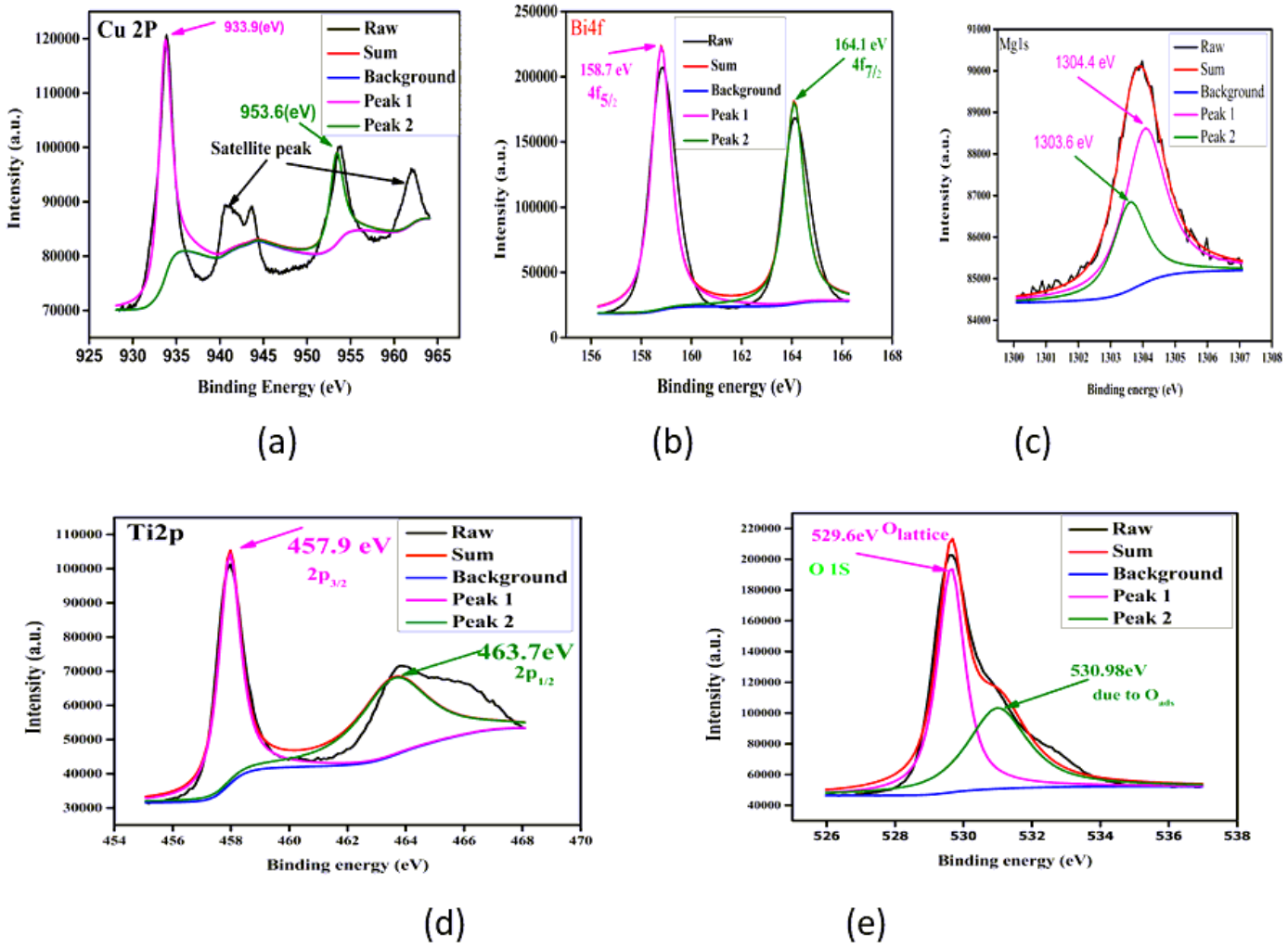

Figure 4

XPS spectra of (a) Cu (b) Bi (c) Mg (d) Ti (e) O of BCMgTO-0.2 ceramic sintered at 1173 K for 8 h.

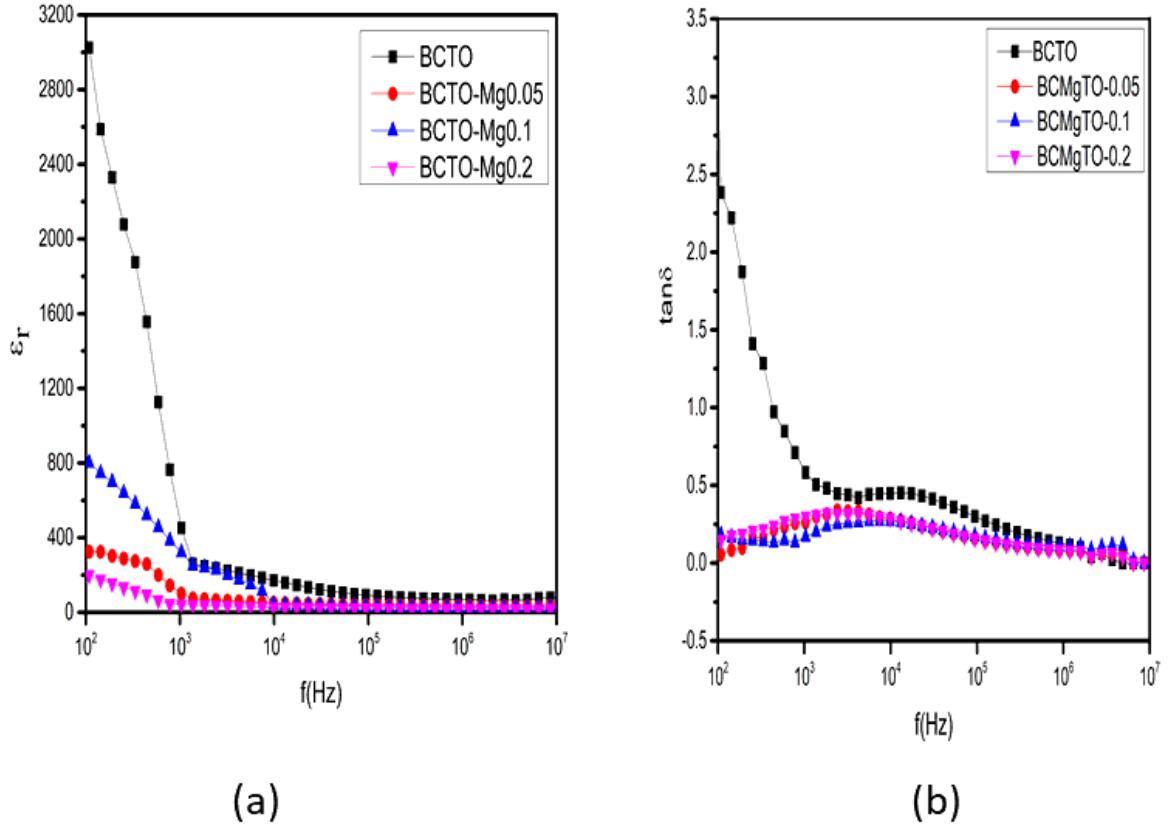

Figure 5

Frequency dependence of (a) dielectric constant(εr) and (b) dielectric loss (tanδ) for BCTO, BCMgTO-0.05, BCMgTO-0.1 and BCMgTO-0.2 ceramics sintered at 1173 K for 8 h.

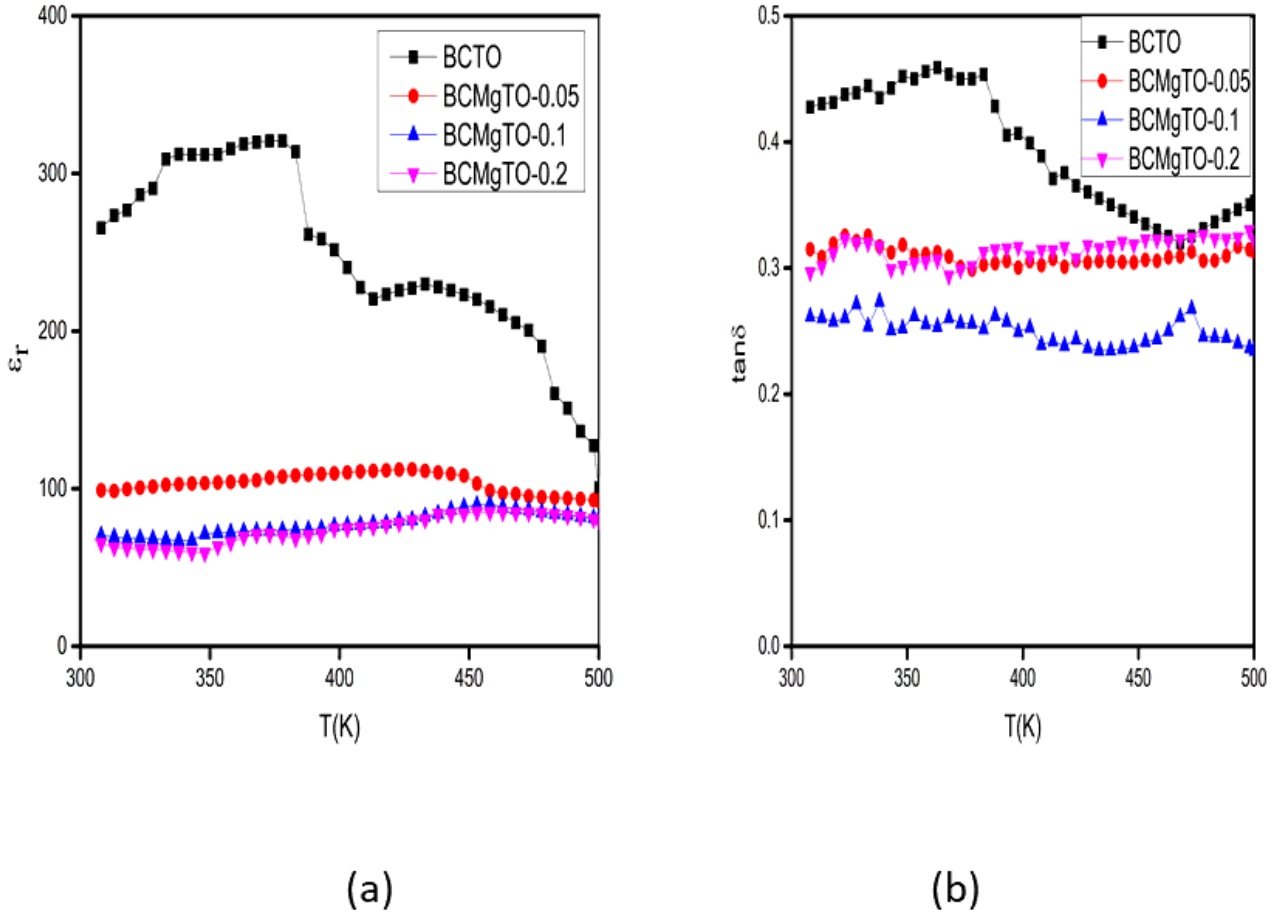

Figure 6

Temperature dependence of (a) dielectric constant(εr) and (b) tangent loss (tanδ) of BCTO, BCMgTO-0.05, BCMgTO-0.1 and BCMgTO-0.2 ceramics sintered at 1173 K for 8 h.

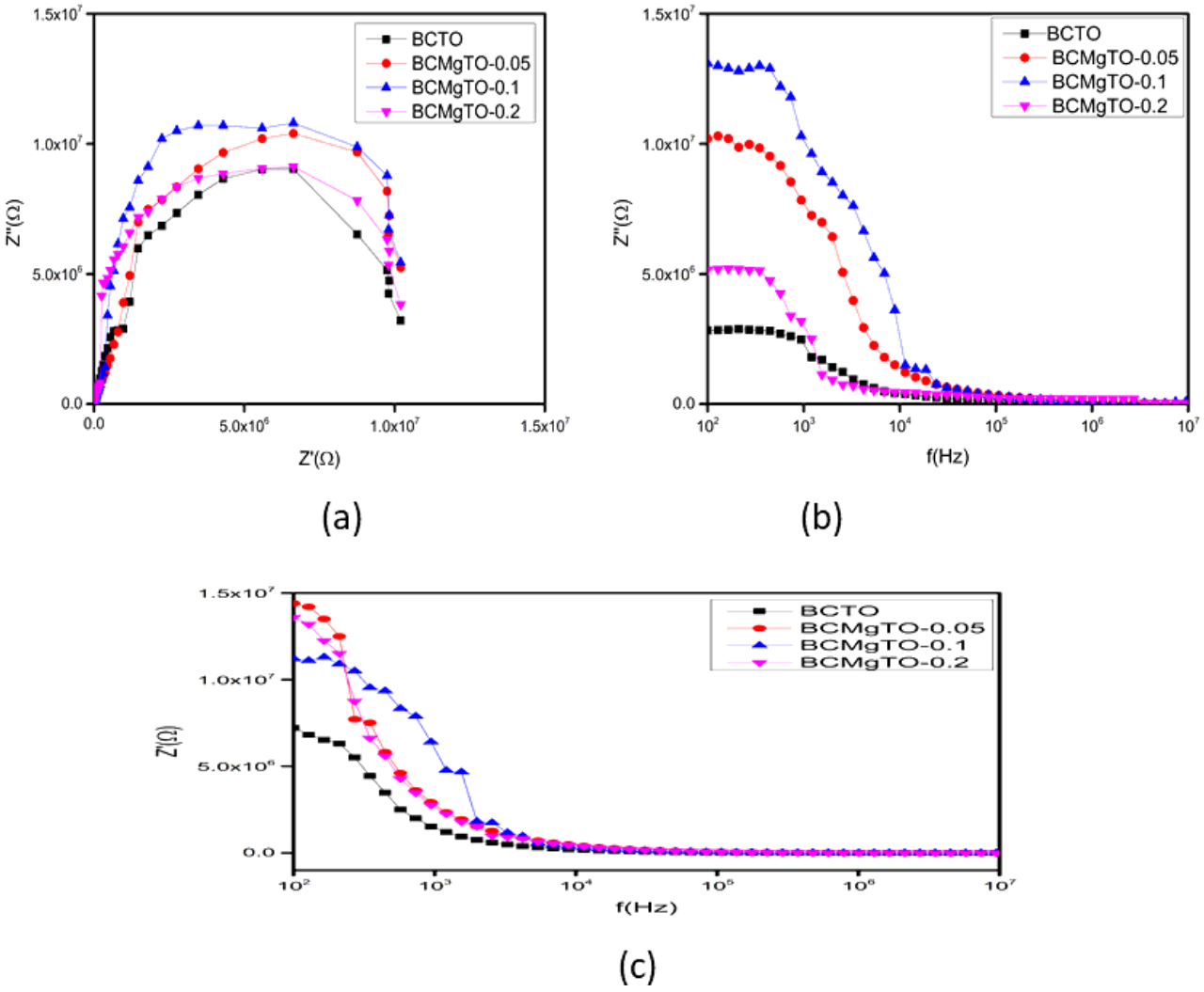

Figure 7

(a) Complex impedance plot or cole-cole plot (Z" vs Z'),(b) frequency dependence of imaginary part of impedance (Z") and (c) frequency dependence of real part of impedance(Z') at 303 K for BCTO, BCMgTO-0.05, BCMgTO-0.1, and BCMgTO-0.2 ceramics.

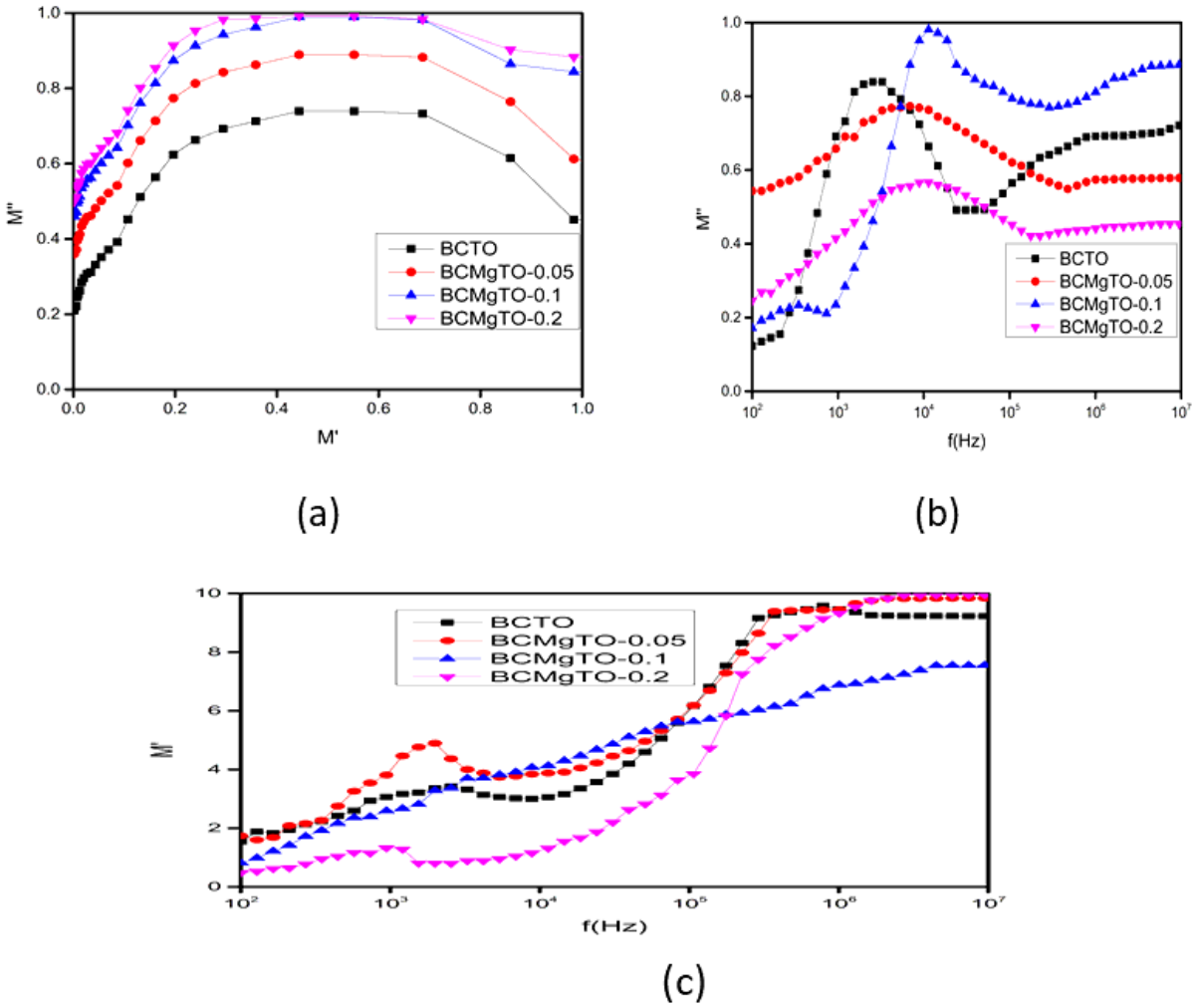

Figure 8

(a) complex electric modulus or Cole-Cole plot(M” vs M’),(b) Frequency dependence of imaginary part of electric modulus(M”) and (c) Frequency dependence of real part of electric modulus(M’) at 303 K for BCTO, BCMgTO-0.05, BCMgTO-0.1, and BCMgTO-0.2 ceramics.

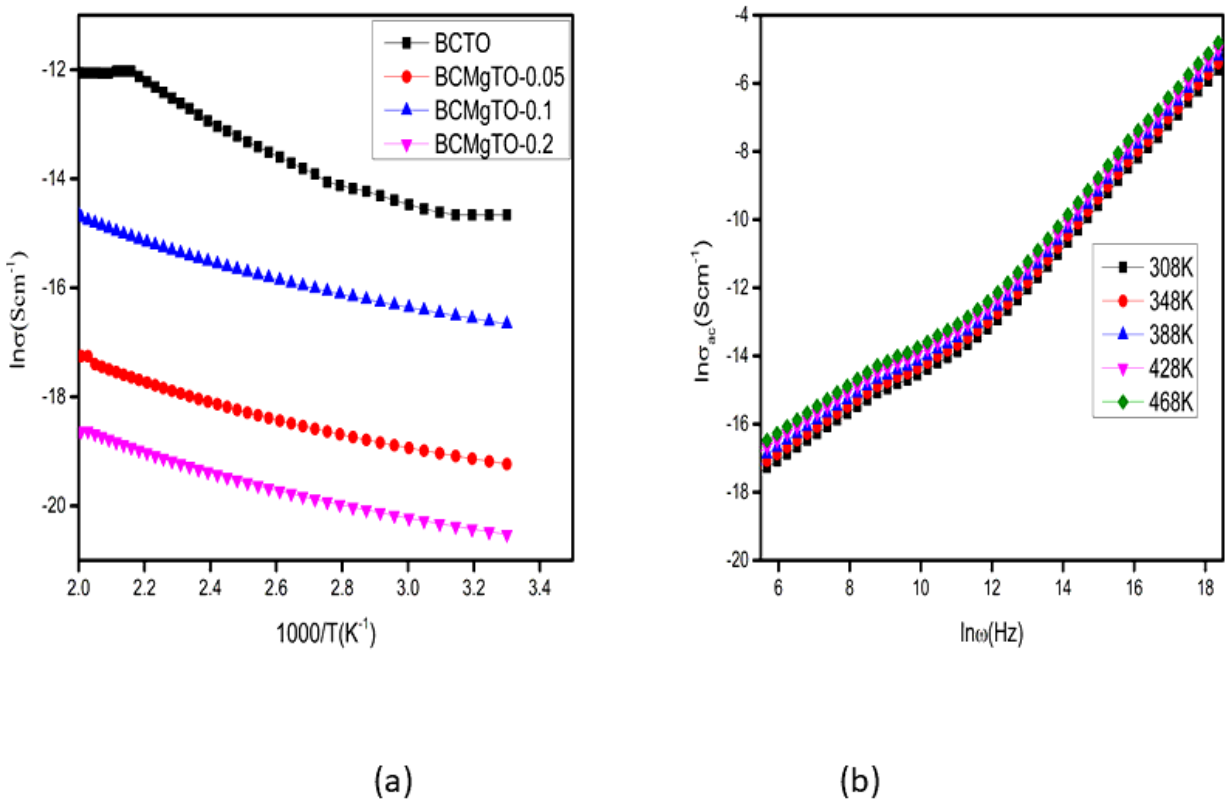

Figure 9

(a) plots of conductivity(lnσ) with the inverse of temperature at 10 kHz and (b) frequency dependence of AC conductivity at 303 K for BCTO, BCMgTO-0.05, BCMgTO-0.1, and BCMgTO-0.2 ceramics.